JTTEE5 19:168–177
DOI: 10.1007/s11666-009-9372-8
1059-9630/$19.00 © ASM International

Influence of TGO Composition on the Thermal Shock Lifetime of Thermal Barrier Coatings with Cold-sprayed MCrAlY Bond Coat

Yong Li, Chang-Jiu Li, Qiang Zhang, Guan-Jun Yang, and Cheng-Xin Li

(Submitted April 22, 2009; in revised form July 16, 2009)

NiCoCrAlTaY bond coat was deposited by cold spraying to assemble thermal barrier coatings (TBCs). The microstructure of the cold-sprayed bond coat was examined using scanning electron microscopy. TBCs consisting of cold-sprayed bond coat and plasma-sprayed YSZ were pretreated at different conditions to form different thermally grown oxides (TGOs) before thermal cycling test. The influence of the TGO composition on the thermal cyclic lifetime was quantitatively examined through the measurement of the coverage ratio of the mixed oxides on the bond coat surface. The results showed that the bond coat exhibited a dense oxidation-free microstructure, and TGOs in different morphologies and constituents were present after thermal cyclic test. The formation of TGOs was significantly influenced by pretreatment conditions. Two kinds of TGO were detected on the surface of bond coat after the spallation of YSZ coatings. One is the α-Al_2O_3-based TGO and the other is the mixed oxide. It was found that the thermal cyclic lifetime is inversely proportional to the coverage ratio of the mixed oxides formed at the bond coat/YSZ interface. The high coverage ratio of the mixed oxide on the interface leads to the early spalling of YSZ coating.

Keywords cold spraying, bond coat, thermal barrier coatings (TBCs), thermally grown oxide (TGO)

1. Introduction

Thermal barrier coatings (TBCs) are widely used in gas turbine for propulsion and power generation (Ref 1-4) due to its ability to reduce the surface temperature of superalloy blades and to prolong the lifetime of blades (Ref 4-6). Constituents in a TBC system include the superalloy substrate, superalloy bond coat, ceramic coating (which is typically yttria-stabilized zirconia, YSZ), and a thermally grown oxide (TGO) formed at the interface between the bond coat and ceramic coating during high temperature operation (Ref 1, 6). Recent investigations (Ref 7-10) revealed that TGO plays an important role in the failure of TBCs.

The thickness of TGO increases with the thermal exposure time following a parabolic law (Ref 1, 11-13). Thickness of TGO determines the stresses within YSZ coating, TGO, and the interface of TGO-bond coat (Ref 1). Rabiei and Evans (Ref 9) observed that the propagation of crack in YSZ coatings moves toward the interface between YSZ coating and TGO with increasing TGO thickness. There exists a critical TGO thickness h_c, below which the delamination of YSZ was exclusively within the TBC. A critical TGO thickness about 5.5 μm was reported (Ref 9). The stress at the TGO-bond coat interface changes with TGO thickness, increasing at convex asperity and concave asperity, according to the simulation of Hsueh and Fuller (Ref 7) based on a three-concentric-circles model. Chen et al. (Ref 14) found that the maximum crack length in YSZ coating increase as a function of TGO thickness. Moreover, the constitutions of the TGO exert different influences on the thermal fatigue behavior.

Four kinds of oxides are generally present in TGO, which are associated with the failure of TBCs in different mechanisms. Those include α-Al_2O_3, Cr_2O_3, NiO, and (Ni, Co)(Cr, Al)$_2O_4$ (Ref 15). A uniform and dense α-Al_2O_3 scale is desirable for its low growth rate (Ref 16). The continuity of α-Al_2O_3 formed at the YSZ/bond coat interface in the pretreatment is critical for the growth of TGO during thermal cycling. A discontinuous α-Al_2O_3

This article is an invited paper selected from presentations at the 2009 International Thermal Spray Conference and has been expanded from the original presentation. It is simultaneously published in *Expanding Thermal Spray Performance to New Markets and Applications: Proceedings of the 2009 International Thermal Spray Conference*, Las Vegas, Nevada, USA, May 4-7, 2009, Basil R. Marple, Margaret M. Hyland, Yuk-Chiu Lau, Chang-Jiu Li, Rogerio S. Lima, and Ghislain Montavon, Ed., ASM International, Materials Park, OH, 2009.

Yong Li, Chang-Jiu Li, Qiang Zhang, Guan-Jun Yang, and **Cheng-Xin Li**, State Key Laboratory for Mechanical Behavior of Materials, School of Materials Science and Engineering, Xi'an Jiaotong University, Xi'an, Shaanxi 710049, P.R. China. Contact e-mail: licj@mail.xjtu.edu.cn.

scale results in the formation of other oxides which exhibit a weak protection to the underlying alloy coating (Ref 17). Cr_2O_3, being a protective scale against oxidation, is usually formed in a relatively high oxygen partial pressure when compared with the formation of α-Al_2O_3 (Ref 14). It protects the underlying alloy from oxidation only at low temperature environment (Ref 18). NiO easily forms in an atmosphere with high oxygen partial pressure. Maier et al. (Ref 19) reported that the parabolic rate constant for NiO scales growing in air at 1100 °C, for example, is typically three orders of magnitude higher than that of the protective α-Al_2O_3. The high growth rate of NiO easily introduces a high level of stress to the TBC system. The most undesirable oxide at the YSZ/bond coat interface is spinel that is usually stoichiometrically expressed as (Ni, Co)(Cr, Al)$_2O_4$ (Ref 16). Its growth is usually accompanied with local and rapid volume increase. Among those oxides, α-Al_2O_3 exhibits a better adhesion to YSZ coating than other three oxides, and spinels are porous, brittle, lacking of capability in antioxidation (Ref 20). In literature (Ref 15, 21-24), the Cr_2O_3, NiO, and spinel are generally referred as mixed oxides. The depletion of Al in bond coat is one of the main reasons for the formation of the mixed oxides (Ref 15, 17, 25).

Many investigators have confirmed qualitatively the deteriorative effect of the mixed oxides on the durability of TBCs (Ref 9, 23, 26). However, it is still not clearly understood quantitatively how the mixed oxides within the TGO affect the durability of TBCs.

It is known that the formation of different oxides on the surface of a bond coat is influenced by its compositions and microstructure which are dependent on preparation process of a bond coat. Low pressure plasma spraying (LPPS) and high velocity oxy-fuel (HVOF) spraying have been widely employed to prepare bond coat (Ref 14, 27-29). The typical feature of these processes is that a bond coat is deposited usually by semi-melted spray droplets. The splashing of partially melted droplets on impact modifies the surface condition of deposited particles from its starting state. Moreover, inevitable oxidation during HVOF modifies the compositions of deposit from the starting powder (Ref 27, 28). On the other hand, with recently developed cold spraying, the compositions and microstructure of superalloy feedstock powders and surface morphology of powder particles as well may be retained into bond coat (Ref 30). This makes cold spraying to be a promising process to deposit superalloy as a bond coat.

In order to understand the performance of cold-sprayed bond coat during high-temperature cycling, in this study, TBCs were prepared consisting of cold-sprayed MCrAlY bond coat and plasma-sprayed YSZ coatings, and thermal cycling test was performed. TBCs were subjected to annealing treatment under different conditions to control TGOs with different contents of spinel and Cr_2O_3. TBCs were subjected to thermal cyclic test till failure of the TBCs, and the influence of the mixed oxides content on the lifetime of TBCs was quantitatively examined in terms of the coverage ratio on the bond coat. The effect of the mixed oxide growth on the failure of atmospheric plasma-sprayed ceramic top coat was discussed.

2. Experimental Procedures

2.1 Materials and Coating Deposition Methods

Nickel-based superalloy (Mar-M247) in a disc shape with dimensions of ∅25.4 mm × 3 mm was used as the substrate. The nominal compositions of the spray powder for bond coat are Ni23Co20Cr8.5Al4Ta0.6Y (−37 μm, Amdry 997, Sulzer Metco Inc., New York, USA), exhibiting a spherical morphology as shown in Fig. 1(a). The 8 wt.% yttria-stabilized zirconia (8YSZ) hollow spheroidized powder (−75 + 45 μm, Metco 204B-NS, Sulzer Metco Inc., New York, USA), shown in Fig. 1(b), was employed to prepare YSZ top coating.

A cold spray system (CS-2000, Xi'an Jiaotong University, China) and an atmospheric plasma spraying (APS) system (GP-80, Jiujiang, and 80 kW Class) were employed to deposit the bond coat and the YSZ top coat,

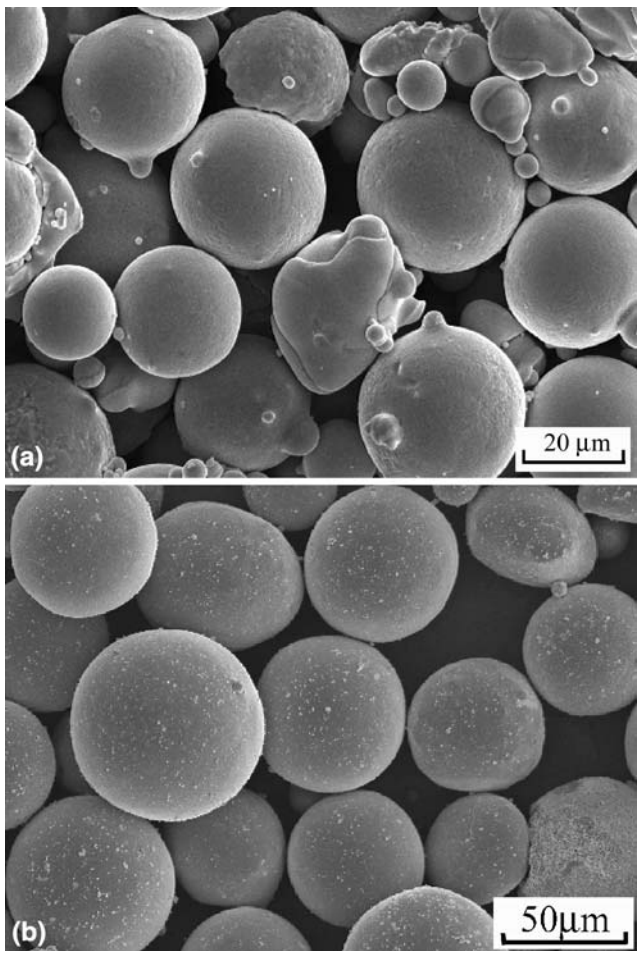

Fig. 1 SEM images of (a) NiCoCrAlY powder for bond coat and (b) 8YSZ powder for top coat

respectively. During cold spraying, helium was employed as the accelerating and powder feeding gas at 2.0 and 2.6 MPa, respectively. The temperature of the accelerating gas was maintained at 580 ± 20 °C during cold spraying. The feeding rate of powder particles was 27.4 g/min. The spray gun traversed at a speed of 150 mm/s with a spray distance of 20 mm. During plasma spraying, argon and hydrogen were used as the primary plasma operating gas and secondary gas, respectively. Argon was used at a pressure of 0.8 MPa and a flow rate of 30 L/min. Hydrogen was used at a pressure of 0.4 MPa and a flow rate of 0.5 L/min. Nitrogen was used as the powder feeding gas at a pressure of 0.1 MPa and a flow rate of 0.25 L/min. Spray distance was fixed at 80 mm. Plasma jet was generated at a plasma arc power of 39 kW.

2.2 Pretreatment and Thermal Cyclic Test for TBCs

Thermal shock test was carried out under a thermal cycling at 1150 °C with a 27-min hold and cooling down to room temperature in 4 min. The failure of the TBCs was defined as 50% of the YSZ coating delaminated and/or spalled. Before the thermal cyclic test, the TBCs samples were subjected to various heat treatments after the deposition of YSZ coating, as shown in Table 1, to introduce various types of TGOs at the YSZ/bond coat interface.

2.3 Measurement of the Content of the Mixed Oxides

The content and distribution of the spinel and Cr_2O_3 along the bond coat/YSZ interface influences significantly the thermal cyclic behavior. The coverage ratio of these mixed oxides on the bond coat after YSZ spalling was estimated based on the scanning electron microscope (SEM, VEGA II-XMU, TESCAN, Czech) image in the backscattered electron image (BEI) mode. On a bond coat surface area with YSZ spalling, nine pictures were taken with 500-μm intervals in two orthogonal directions, respectively. Twenty-seven pictures were taken on three areas for each specimen. Through image processing based on the contrast among spinel, Cr_2O_3, and Al_2O_3 on the BEI, the coverage ratio of the mixed oxide was estimated, which is defined as the ratio of the covered areas by the mixed oxides on the bond coat surface to the whole areas of the image.

Table 1 Pretreatment conditions of TBC samples

Treatment types	Treatment details
Type-1	1080-1160 °C for 4 h in Ar (ramping)
Type-2	1080-1160 °C for 4 h in Ar (oven preheated)
Type-3	1080-1160 °C for 4 h in Ar (ramping) + 1000-1080 °C for 10 h in air
Type-4	1150 °C for 30 min in air (oven preheated) + 1080-1160 °C for 4 h in Ar (oven preheated)

3. Results and Discussion

3.1 Microstructure of the As-Deposited TBC

Figure 2(a) shows the microstructure of the as-deposited TBCs. The bond coat exhibited a dense microstructure, and

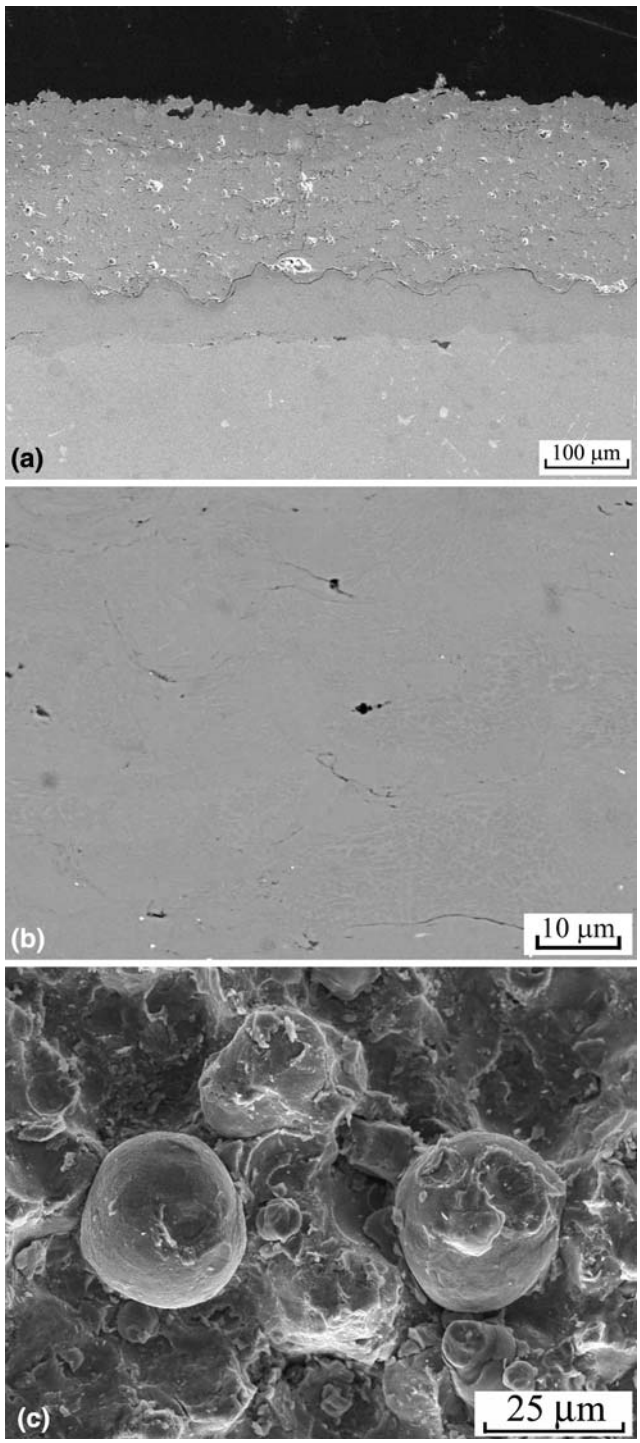

Fig. 2 Microstructure of the as-deposited TBC (a), the as-deposited bond coat (b), and the surface morphology of bond coat (c)

no evident oxidation was observed during coating deposition. Limited pores were present in the bond coat, as shown in Fig. 2(b). The dense microstructure was attributed to the successive impacting of solid particles at a high velocity. It can be observed that the amount of internal oxide stringers, and pores in the bond coat deposited by APS (Ref 27) or HVOF technique (Ref 28, 29) can be considerably reduced by employing cold spraying process. When compared with the bond coat deposited by LPPS (Ref 28), no evident difference can be observed on cross-sectional microstructure. However, it was noticed that cold-sprayed alloy coat presents a much different surface morphology from any other bond coat deposited by thermal spray process, such as the LPPS/VPS (vacuum plasma spraying), HVOF, and APS. The cold spray bond coat may retain locally the spherical smooth surface morphology (Fig. 2c). On the other hand, the splashing of liquid particle fraction during droplet impact during conventional thermal spray deposition may lead to the bond coat surface to be in a highly irregular morphology, which can be clearly observed in the results reported in the literature (Ref 31, 32). Accordingly, oxidation and thermal cyclic behavior of cold-sprayed bond coat may be largely different from the bond coat deposited by thermal spray processes due to the different morphologies according to the results supplied by Haynes et al. (Ref 33).

3.2 Characteristics of TGO After Pretreatment

Figure 3 shows the typical microstructure and surface morphology of TGOs evolved on the cold-sprayed bond coat surface during preannealing treatments. A Ni protective layer was deposited on the surface prior to the preparation of the sample for examination of cross-sectional microstructure by electroless plating. Figure 3(a) and (b) show these of TGOs observed when bond coat was pretreated at the Type-1 condition. A uniform continuous TGO was formed (Fig. 3a), while the surface morphology indicated that in some local places, especially in the region of the concavity, needle-like alumina which is proposed as the theta alumina (Ref 34) was observed (Fig. 3b). Such needle-like theta alumina was possibly formed at low-temperature range during heating up of the sample. The TGOs on the bond coat surfaces pretreated at Type-2 and

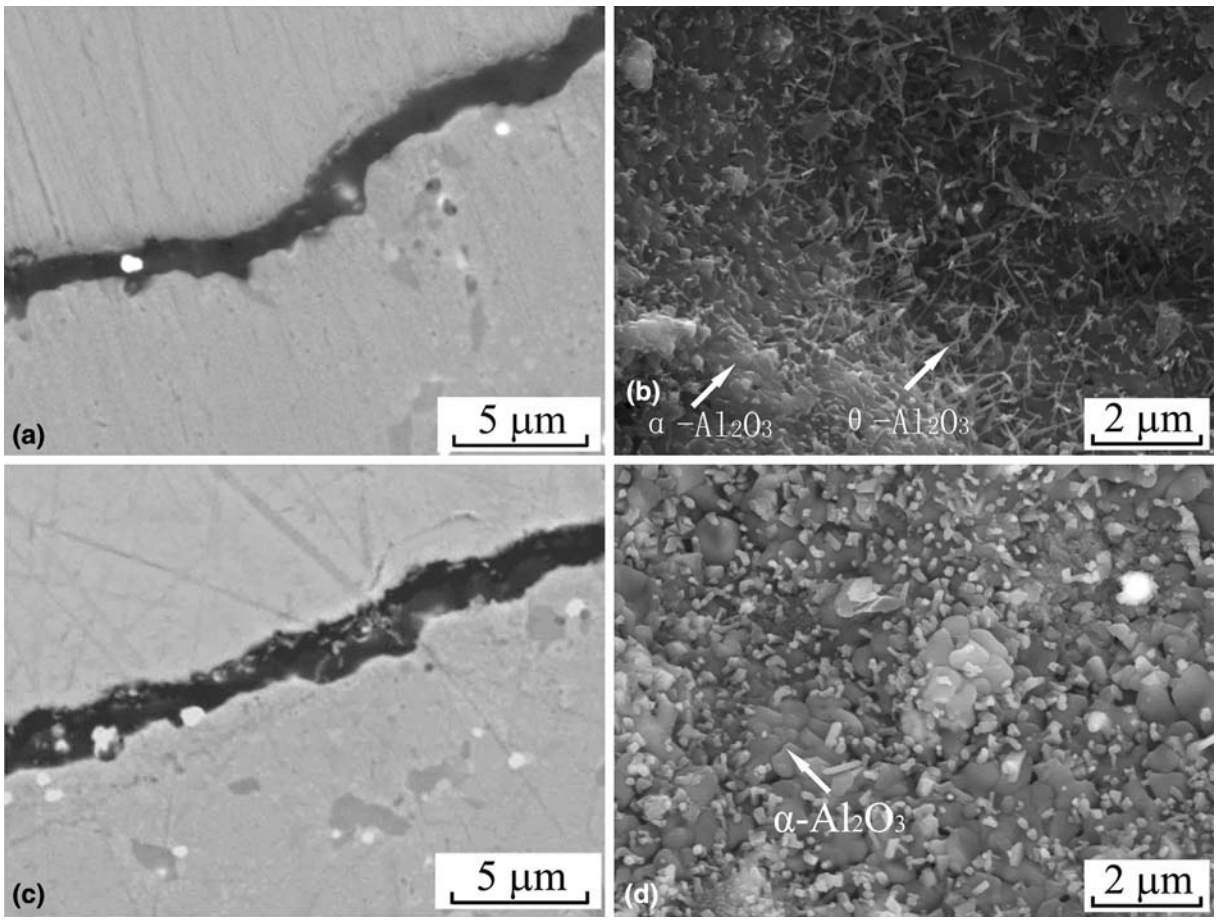

Fig. 3 Cross-sectional microstructure and surface morphology of TGOs evolved under different pretreatments. (a, c, e) and (g-h) show the microstructure of TGOs formed at Type-1, Type-2, Type-3, and Type-4 conditions, respectively; (b), (d), and (f) show the surface morphology of the TGOs formed at Type-1, Type-2, and Type-3 conditions, respectively. The cross-sectional microstructure was observed at BSE mode and the surface morphology was observed at SEM mode

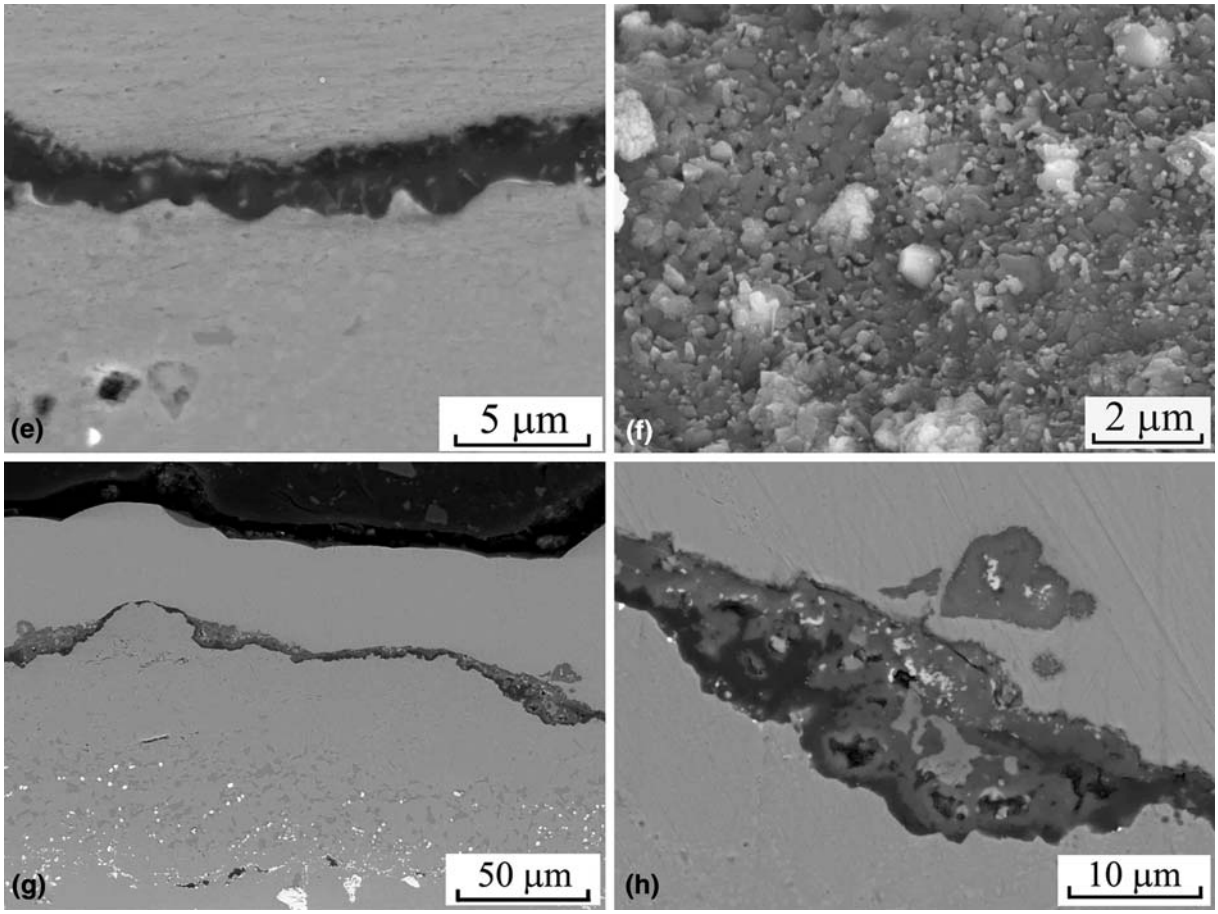

Fig. 3 Continued

Type-3 conditions exhibited a morphology of an exclusive and uniform α-Al_2O_3, as showed by Fig. 3(c-f). Moreover, it was observed that the thickness of TGO formed at the Type-3 conditions was statistically a little thicker than that of Type-2 and Type-1 due to longer exposure time to oxidation atmosphere during pretreatment.

However, TGO on the bond coat pretreated at the Type-4 condition exhibited a different morphology and composition from the Type-1 to Type-3 as can be seen from Fig. 3(g) and (h). It is clear that porous and large TGO in volume covered the surface of the bond coat after preoxidation of cold-sprayed bond coat. Such TGO was composed of the mixed oxides of spinel and Ni/Cr oxides. On the other hand, it can be clearly observed that the bond coat presents a much dense microstructure without splat interfaces after heat treatment. This is because the oxidation-free feature of cold-sprayed coating promotes the element diffusion at the interfaces between splats in the coating during high-temperature treatment. Moreover, evidently the dense microstructure feature of the cold-sprayed coating prevented the coating from the inner oxidation even it was exposed directly to high-temperature oxidation atmosphere in air as in Type-4 treatment. It was also observed that the phase in white contrast was precipitated in the bond coat during pretreatment, which are dispersed in the grain boundaries in the bond coat. The EDS analysis confirmed this phase to be Ta-rich one.

The above results clearly show that with cold-sprayed MCrAlY bond coat, the different preoxidation conditions may lead to formation of TGOs with different morphology and compositions. It was confirmed that the direct exposure of cold-sprayed NiCoCrAlTaY coating at high temperature of 1150 °C in air results in formation of the oxide mainly composed of spinel with a high growth rate.

3.3 The Constituents and Characteristics of TGO in the Failed TBCs

The examination of the TGO from the cross section and surface of the failed TBC samples after the thermal shock test revealed that three different types of oxides including spinel-based oxide, Cr_2O_3-based oxide, and α-Al_2O_3-based oxide were formed along the cold-sprayed bond coat/YSZ interface as shown in Fig. 4.

The TGOs, shown in Fig. 4(a-d), were present at the bond coat/YSZ interface as large protrusions which were mainly composed of spinel and Cr_2O_3, being referred as the mixed oxides. It was observed (Fig. 4a) that cracks propagated through the porous spinel. The Cr_2O_3-based

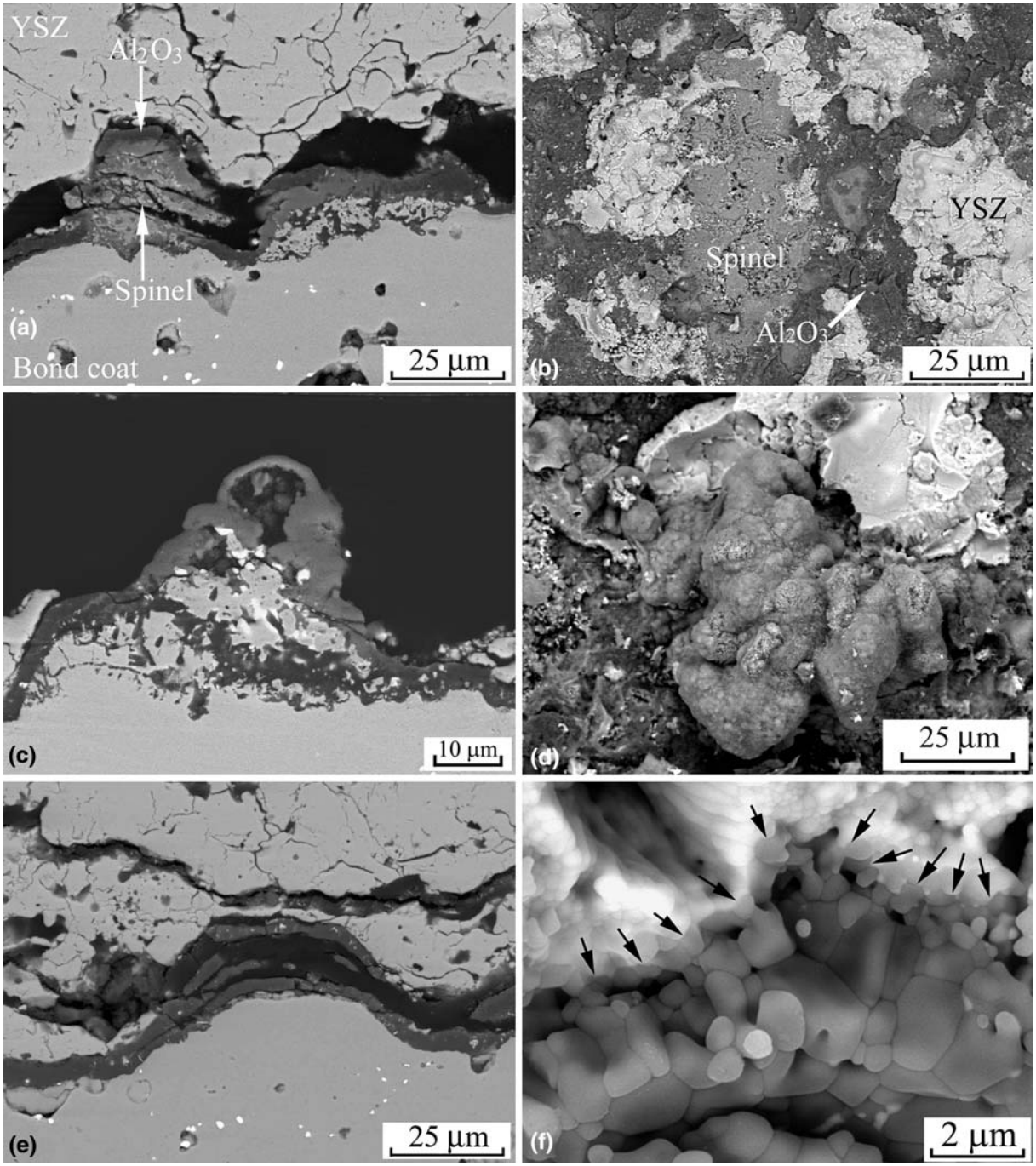

Fig. 4 Three types of TGOs after thermal cyclic test and the corresponding crack propagation style. (a) Spinel through which crack propagated, 84 cycles. (b) A fractured surface after YSZ spalled in the spinel, 84 cycles. (c) Cr_2O_3, crack propagated along the interface between Cr_2O_3 and YSZ, 84 cycles. (d) An irregular surface of the Cr_2O_3, 6 cycles. (e) The multilayered α-Al_2O_3, 213 cycles. (f) The adherence between grains of YSZ and α-Al_2O_3 pointed by black arrows, 435 cycles

oxide was detached from the interface between the YSZ and the TGO (Fig. 4c), which means that the Cr_2O_3-based oxide was adhered weakly to the YSZ coating.

On the other hand, the α-Al_2O_3-based TGO was continuous and uniform in thickness at the troughs of the interface. However, α-Al_2O_3 at the undulation crest was several times thicker than that of the TGO at troughs and exhibited a multilayered structure, as shown in Fig. 4(e). Cracks in the layered α-Al_2O_3-based TGO were almost parallel to the TGO/BC interface. It was also observed that a layer of Al_2O_3 was attached to the YSZ coating, as shown in Fig. 4(e), which means that the α-Al_2O_3-based TGO was strongly adhered to the YSZ coating. As shown in Fig. 4(f), on the concave surface of the YSZ coating, it

was found that a layer of Al_2O_3 grains was bonded to the YSZ grains. The bonding interface was marked by the black arrows in Fig. 4(f). Therefore, α-Al_2O_3-based TGO is desirable for its excellent protection and adherence to the YSZ coating in comparison to the non-alumina TGO.

3.4 Effect of the Mixed Oxides on the Lifetime of TBCs

3.4.1 The Thermal Cycling Lifetime of TBCs. The thermal cycling lifetime of TBCs is shown in Table 2. Three samples were tested with each pretreatment condition. It was found that the lifetimes of TBCs deposited in this study were distributed in a large range from 6 to 435 cycles. With the Type-4 treatment, TBCs samples only exhibited lifetimes from 6 to 26 cycles. The lifetime is less than one-tenth of the maximum in this study. With the pretreatments under Type-2 and Type-3, most samples exhibited lifetime around 200 cycles. However, it was found that three samples exhibited a lifetime over 300 cycles and even over 400 cycles. Qualitatively, the different thermal cyclic lifetime is attributed to the development of different types of TGOs at the interface between bond coat and YSZ. It is known that a fast grown spinel would be deteriorative to failure of TBCs. To reveal the origin of such different thermal cyclic lifetimes, the relationship between the mixed oxides content and the lifetime of TBCs is quantitatively examined as shown in the following section.

3.4.2 Relationship Between the Content of Mixed Oxides and Lifetimes. The examination of the effect of TGO on the cracking of the YSZ coating indicated that the mixed oxides of spinel and Cr_2O_3 are deteriorative to the lifetime of TBCs. The examination of the TBCs failure models revealed that the premature failure is directly associated to the TGO compositions. Formation of spinel and Cr_2O_3 was fatal to the lifetime of TBCs. The surface coverage ratio of the mixed oxides consisted of both spinel and Cr_2O_3 formed on the bond coat surface after the sample failure was estimated. As shown in Fig. 5, it was clear that with the increase of the surface coverage of spinel and Cr_2O_3, the thermal cyclic lifetime decreased rapidly. An improved thermal cyclic lifetime was associated to the reduced spinel and Cr_2O_3 coverage ratio. With thermal cyclic lifetime being longer than 168 cycles, the growth of the multilayered α-Al_2O_3 dominated the failure of TBCs, instead of the spinel and Cr_2O_3, as shown in Fig. 6. In the failed TBCs with a lifetime of over 400 cycles, almost no spinel and evident Cr_2O_3 was observed. Therefore, to prevent the mixed oxide formation during thermal cyclic test is critical to improving the cyclic lifetimes of the TBCs.

Table 2 The thermal cycling lifetime of TBCs

Treatment types	Thermal cyclic lifetimes
Type-1	84, 144, 434
Type-2	168, 195, 301
Type-3	213, 185, >400
Type-4	6, 19, 26

3.4.3 Effect of Mixed Oxide on the Stability of YSZ Coatings. Figure 7 shows the typical cracks between the bond coat and the survived YSZ after thermal shock test. Two types of cracks (Fig. 7a) were present in the YSZ coating and the YSZ/TGO interface, respectively. Evidently, such cracks originated from the tip of the TGO and propagated along the lamellar interface in the YSZ coating. The growth of the TGO at the interface between the YSZ and bond coat (Fig. 7b) causes the localized expansion which exerts the additional tension to the YSZ surrounding the oxide. When the intensity of the tension exceeds the cohesive strength of the YSZ lamellae, the crack will propagate into the bonded interface area along the nonbonded interface area between the lamellae and possibly into the nonmolten

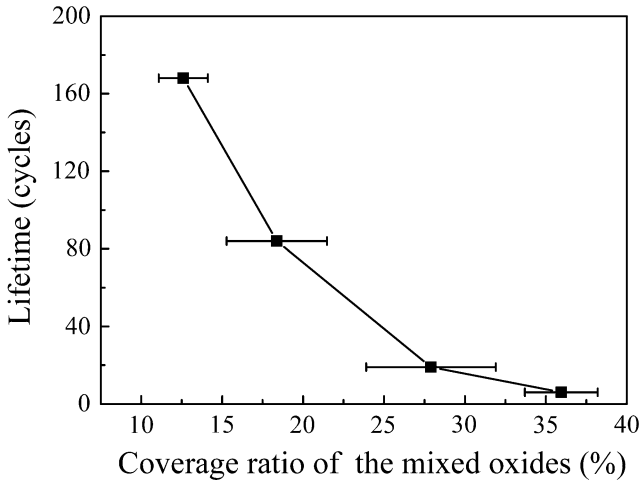

Fig. 5 Relationship between the surface coverage of the mixed oxides on the bond coat surface and thermal cyclic lifetime after TBC failure

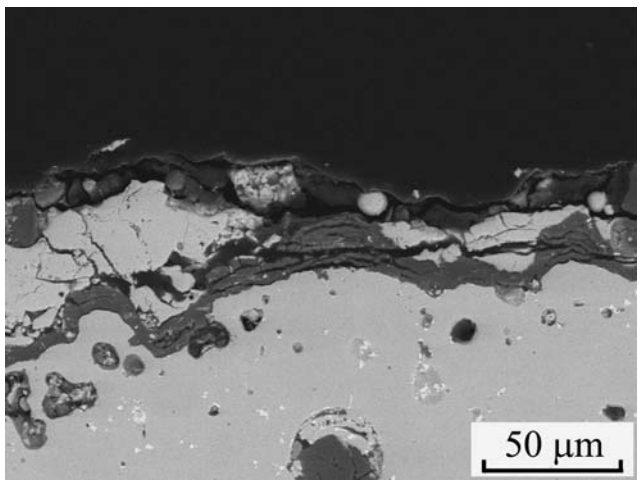

Fig. 6 A typical cross section of TBC sample experienced 435 thermal cycles demonstrating the failure caused by the growth of a layered alumina

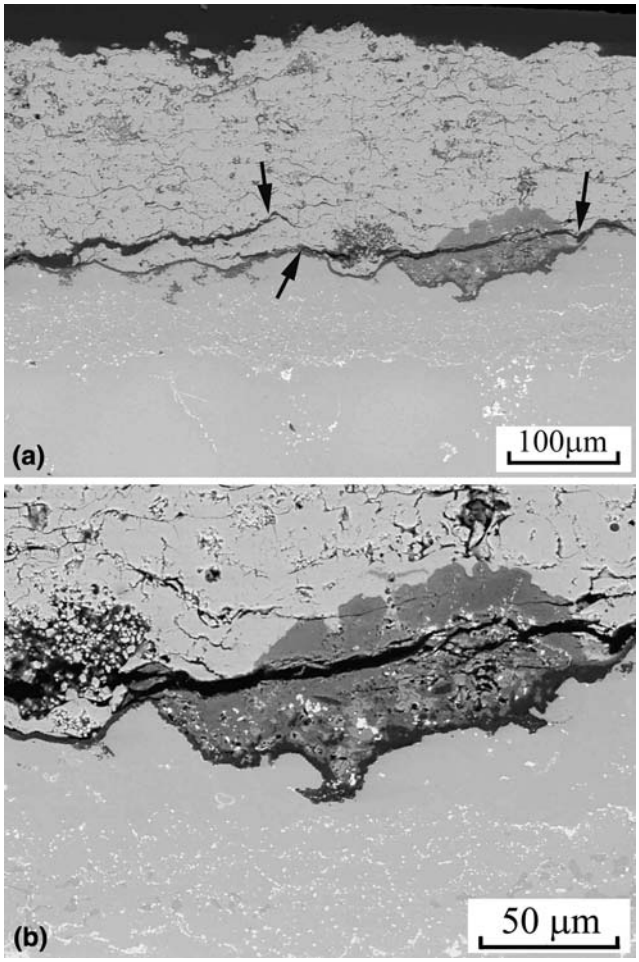

Fig. 7 (a) Cracks which are supposed to be induced by mixed TGO, lifetime: 19 cycles and caused by the growth of mixed oxide; (b) a closer view on the mixed oxides and cracks surrounding it

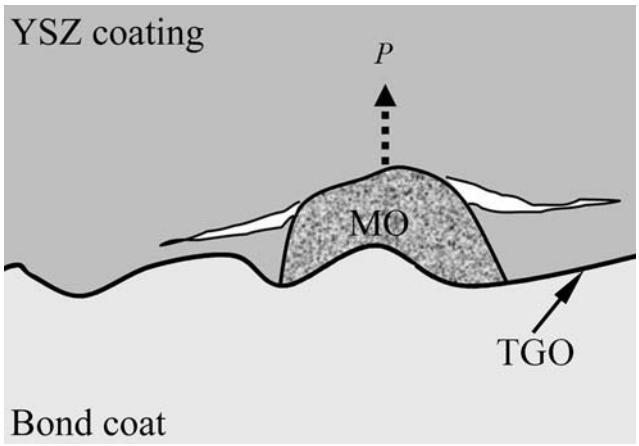

Fig. 8 A schematic diagram to show the cracking style of the YSZ coating near the undulation troughs. MO stands for the mixed oxide

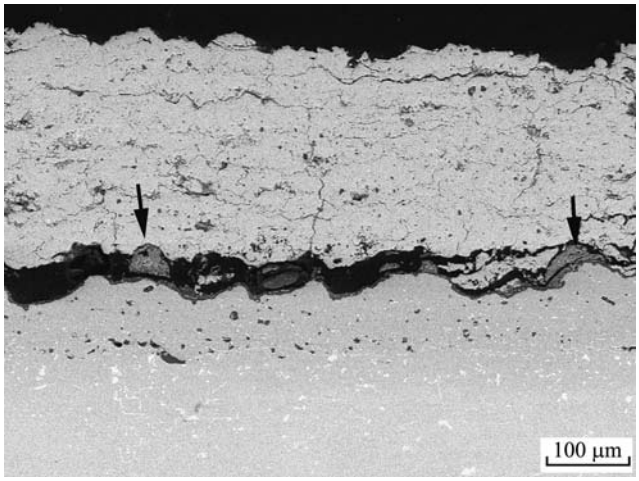

Fig. 9 Typical cross-sectional microstructure of TBC experienced 84 thermal cycles to show the bridging of the cracks between two neighboring mixed oxides

YSZ porous particles (Fig. 7b), which may cause the spalling of the YSZ from the TGO. Cracks propagation induced by the mixed oxides terminated after cracks propagated to certain distance propagation, as shown in Fig. 7(a) marked by the black arrows.

A model, as shown in Fig. 8, was proposed based on Fig. 7 to elaborate the effect of mixed oxide on the YSZ coating. In this model, P stands for the compressive force, acting on the YSZ coating by the local protruding TGO (MO) including the abovementioned three oxides at the YSZ/bond coat interface. The magnitude of this compressive force is determined by the growth rate of TGO. The higher the growth rate the higher the compressive force. The alumina-based TGO with the lowest growth rate introduced the smallest compressive force among various TGOs. On the other hand, plasma-sprayed YSZ coating shows a lamellar microstructure with a limited interface bonding (Ref 35). The nonbonded areas are virtually present in the coating as the cracks parallel to the interface of the YSZ coating/bond coat which reduce the thermal conductivity (Ref 36-38) and the toughness of the YSZ coating at the direction parallel to the surface of the YSZ coating (Ref 35, 39). The crack propagation will be initiated through the YSZ coating with a low toughness by the tensile force P, being the compressive stress exerted by the growth of protruding TGO, as illustrated by the model. With the growth of the local protruding TGO, the length of cracks is increased. However, the propagation of cracks stops as the stress and associated strain energy density is alleviated where the effect by the growth of the MO becomes much limited. The propagation style of cracks caused by the single protrusion is much the same as that in Obreimoff experiment (Ref 40). The length of cracks caused by a single protruding TGO is limited when the spacing of neighboring protrusions is large. However, the growth of large number of protruding TGOs at the YSZ/bond coat interface, as pointed by arrows in Fig. 9,

causes the bridging of cracks. The delamination of the YSZ coating from the bond coat was resulted from the bridging of the crack propagation induced by the growth of protrusions.

4. Conclusions

Thermal cyclic test was employed to evaluate the lifetime of TBCs pretreated in different conditions. The TBCs consisted of a dense cold-sprayed NiCoCrAlTaY bond coat without oxidation during spraying. The results showed that oxidation behavior of the cold-sprayed bond coat can be significantly influenced by preoxidation conditions, which further significantly influence the thermal cyclic lifetime of TBCs. Three types of TGOs including spinel, Cr_2O_3, and multilayered α-Al_2O_3 were detected. Spinel was brittle and porous. Chrome oxide exhibited a weak adhesion to YSZ coating. α-Al_2O_3-based TGO exhibited a strong bonding to the YSZ coating. The direct exposure of cold-sprayed bond coat to air at a high temperature of 1150 °C led to the formation of fast grown spinel-based mixed TGO at the interface between the bond coat and YSZ. It was quantitatively revealed that the thermal cyclic lifetime was inversely proportional to the coverage ratio of the mixed oxides formed at the bond coat/YSZ interface. The high coverage of the mixed oxide on the interface led to the early spalling of the YSZ coating. The local growth of the mixed oxides induced the cracking along the weak-bonded areas between the lamellae in the YSZ coating. Moreover, the results suggest that through controlling of pretreatment condition, the dominant oxide to TBCs failure can be changed from fast grown spinel to exclusive α-Al_2O_3 due to limited oxidation of superalloy bond coat during cold spraying, which led to the increase of thermal cyclic life time even by a factor of 10.

Acknowledgments

The present project was financially support by National Basic Research Program of China (No. 2007CB707702) and National Science Fund for Distinguish Young Scholars (No. 50725101).

References

1. A.G. Evans, D.R. Mumm, J.W. Hutchinson, G.H. Meier, and F.S. Pettit, Mechanisms Controlling the Durability of Thermal Barrier Coatings, *Prog. Mater. Sci.*, 2001, **46**(5), p 505-553
2. W.J. Brindley, Thermal Barrier Coatings, *J. Therm. Spray Technol.*, 1996, **5**(4), p 379-380
3. E. Garcia, P. Miranzo, R. Soltani, and T.W. Coyle, Microstructure and Thermal Behavior of Thermal Barrier Coatings, *J. Therm. Spray Technol.*, 2008, **17**(4), p 478-485
4. Q. Zhang, C.-J. Li, Y. Li, S.-L. Zhang, X.-R. Wang, G.-J. Yang, and C.-X. Li, Thermal Failure of Nanostructured Thermal Barrier Coatings with Cold-Sprayed Nanostructured NiCrAlY Bond Coat, *J. Therm. Spray Technol.*, 2008, **17**(5-6), p 838-845
5. I.G. Wright and T.B. Gibbons, Recent Developments in Gas Turbine Materials and Technology and Their Implications for Syngas Firing, *Int. J. Hydrog. Energy*, 2007, **32**(16), p 3610-3621
6. N.P. Padture, M. Gell, and E.H. Jordan, Thermal Barrier Coatings for Gas-Turbine Engine Applications, *Science*, 2002, **12**(296), p 280-284
7. C.H. Hsueh and E.R. Fuller, Jr., Analytical Modeling of Oxide Thickness Effects on Residual Stresses in Thermal barrier, *Scripta Mater.*, 2000, **42**(8), p 781-787
8. F. Tang and J.M. Schoenung, Local Accumulation of Thermally Grown Oxide in Plasma-Sprayed Thermal Barrier Coatings with Rough Top-Coat/Bond-Coat Interfaces, *Scripta Mater.*, 2005, **52**(9), p 905-909
9. A. Rabiei and A.G. Evans, Failure Mechanisms Associated with the Thermally Grown Oxide in Plasma-Sprayed Thermal Barrier Coatings, *Acta Mater.*, 2000, **48**(15), p 3963-3976
10. K.W. Schlichting, N.P. Padture, E.H. Jordan, and M. Gell, Failure Modes in Plasma-Sprayed Thermal Barrier Coatings, *Mater. Sci. Eng. A*, 2003, **342**(1-2), p 120-130
11. H. Iwamoto, T. Sumikawa, K. Nishida, T. Asano, M. Nishida, and T. Araki, High Temperature Oxidation Behavior of Laser Clad NiCrAlY Layer, *Mater. Sci. Eng. A Struct.*, 1998, **241**(1-2), p 251-258
12. W. Brand, H.J. Grabke, D. Toma, and J. Kriiger, The Oxidation Behaviour of Sprayed MCrAlY Coatings, *Surf. Coat. Technol.*, 1996, **86-87**(Part 1), p 41-47
13. I. Spitsberg and K. More, Effect of Thermally Grown Oxide (TGO) Microstructure on the Durability of TBCs with PtNiAl Diffusion Bond Coats, *Mater. Sci. Eng. A Struct.*, 2006, **417**(1-2), p 322-333
14. W.-R. Chen, R. Archer, X. Huang, and B.R. Marple, TGO Growth and Crack Propagation in a Thermal Barrier Coating, *J. Therm. Spray Technol.*, 2008, **17**(5-6), p 858-864
15. K. Ogawa, K. Ito, T. Shoji, D.W. Seo, H. Tezuka, and H. Kato, Effects of Ce and Si Additions to CoNiCrAlY Bond Coat Materials on Oxidation Behavior and Crack Propagation of Thermal Barrier Coatings, *J. Therm. Spray Technol.*, 2006, **15**(4), p 640-651
16. M. Matsumoto, K. Hayakawa, S. Kitaoka, H. Matsubara, H. Takayama, Y. Kagiya, and Y. Sugita, The Effect of Preoxidation Atmosphere on Oxidation Behavior and Thermal Cycle Life of Thermal Barrier Coatings, *Mater. Sci. Eng. A Struct.*, 2006, **441**(1-2), p 119-125
17. S. Taniguchi and A. Andoh, Improvement in the Oxidation Resistance of an Al-Deposited Fe-Cr-Al Foil by Preoxidation, *Oxid. Met.*, 2002, **58**(5-6), p 545-562
18. R.-F. Zhou, Y.-F. Han, and S.-S. Li, *High Temperature Structure Materials*, 1st ed., National Dense Industry Press, China (in Chinese)
19. R.D. Maier, C.M. Scheuermann, and C.W. Andrews, Degradation of a Two-layer Thermal Barrier Coating under Thermal Cycling, *Am. Ceram. Soc. Bull.*, 1981, **60**(5), p 555-561
20. V. Teixeira, M. Andritschky, W. Fischer, H.P. Buchkremer, and D. Stöver, Effects of Deposition Temperature and Thermal Cycling on Residual Stress State in Zirconia-based Thermal Barrier Coatings, *Surf. Coat. Technol.*, 1999, **120-121**, p 103-111
21. P. Saltykov, O. Fabrichnaya, J. Golczewski, and F. Aldinger, Thermodynamic Modeling of Oxidation of Al-Cr-Ni Alloys, *J. Alloy. Compd.*, 2004, **381**(1-2), p 99-113
22. W.-R. Chen, X. Wu, B.R. Marple, D.R. Nagy, and P.C. Patnaik, TGO Growth Behaviour in TBCs with APS and HVOF Bond Coats, *Surf. Coat. Technol.*, 2008, **202**(12), p 2677-2683
23. M.S. Ali, S. Song, and P. Xiao, Degradation of Thermal Barrier Coatings due to Thermal Cycling up to 1150°C, *J. Mater. Sci.*, 2002, **37**(22), p 2097-2102
24. O. Trunova, T. Beck, R. Herzog, R.W. Steinbrech, and L. Singheiser, Damage Mechanisms and Lifetime Behavior of Plasma Sprayed Thermal Barrier Coating Systems for Gas Turbines—Part I: Experiments, *Surf. Coat. Technol.*, 2008, **202**(20), p 5027-5032
25. K.A. Khor and Y.W. Gu, Thermal Properties of Plasma-Sprayed Functionally Graded Thermal Barrier Coatings, *Thin Solid Films*, 2000, **372**(1-2), p 104-113

26. K.M. Carling and E.A. Carter, Effects of Segregating Elements on the Adhesive Strength and Structure of the α-Al_2O_3/β-NiAl Interface, *Acta Mater.*, 2007, **55**(8), p 2791-2803
27. W.R. Chen, X. Wu, B.R. Marple, R.S. Lima, and P.C. Patnaik, Pre-oxidation and TGO Growth Behaviour of an Air-plasma-sprayed Thermal Barrier Coating, *Surf. Coat. Technol.*, 2008, **202**(16), p 3787-3796
28. M. Shibata, S. Kuroda, M. Wantanabe, H. Murakami, and M. Ode, Microstructure and Oxidation of MCrAlY Coatings Produced by Various Thermal Spray Process, *Thermal Spray 2007:Building on 100 Years of Success*, On CD-ROM, B.R. Marple, M.M. Hyland, Y.-C. Lau, R.S. Lima, and J. Voyer, Ed., May 15-18, 2007 (Seattle, USA), ASM International, 2006
29. D.B. Lee, J.H. Ko, and J.H. Yi, Characterization of Oxide Scales Formed on High-Velocity Oxyfuel-Sprayed Ni-Co-Cr-Al-Y+ReTa Coatings, *J. Therm. Spray Technol.*, 2005, **14**(3), p 315-320
30. W.-Y. Li, H. Liao, H.-T. Wang, C.-J. Li, G. Zhang, and C. Coddet, Optimal Design of a Convergent-Barrel Cold Spray Nozzle by Numerical Method, *Appl. Surf. Sci*, 2006, **253**(2), p 708-713
31. C. Zhang, H.-L. Liao, W.-Y. Li, G. Zhang, C. Coddet, C.-J. Li, C.-X. Li, and X.-J. Ning, Characterization of YSZ Solid Oxide Fuel Cells Electrolyte Deposited by Atmospheric Plasma Spraying and Low Pressure Plasma Spraying, *J. Therm. Spray Technol.*, 2006, **15**(4), p 598-603
32. R.B. Heimann and T.A. Vu, Low-Pressure Plasma-Sprayed (LPPS) Bioceramic Coatings with Improved Adhesion Strength and Resorption Resistance, *J. Therm. Spray Technol.*, 1997, **6**(2), p 145-149
33. J.A. Haynes, E.D. Rigney, M.K. Ferber, and W.D. Porter, Oxidation and Degradation of a Plasma-Sprayed Thermal Barrier Coating System. *Surf. Coat. Technol.*, 1996, **86-87**(Part 1), 102-108,
34. G.C. Rybicki and J.L. Smialek, Effect of the θ-α-Al_2O_3 Transformation on the Oxidation Behavior of β-NiAl $\pm$ Zr, *Oxid. Met.*, 1989, **31**(3/4), p 275-304
35. A. Ohmori, C.-J. Li, and Y. Arata, Influence of Plasma Spray Conditions on the Structure of Al_2O_3 Coatings, *Trans. Jpn. Weld. Res. Inst.*, 1990, **19**(2), p 99-110
36. R. McPherson, A Model for Thermal Conductivity of Plasma Sprayed Ceramic Coatings, *Thin Solid Films*, 1984, **112**(3), p 89-95
37. F. Cernuschi, P.G. Bison, S. Marinetti, and P. Scardi, Thermophysical, Mechanical and Microstructural Characterization of Aged Free-standing Plasma-sprayed Zirconia Coatings, *Acta Mater.*, 2008, **56**(16), p 4477-4488
38. G. Bertrand, P. Bertrand, P. Roy, C. Rio, and R. Mevrel, Low Conductivity Plasma Sprayed Thermal Barrier Coating using Hollow PSZ Spheres: Correlation Between Thermophysical Properties and Microstructure, *Surf. Coat. Technol.*, 2008, **202**(10), p 1994-2001
39. C.-J. Li, W.-Z. Wang, and Y. He, Dependance of Fracture Toughness of Plasma Sprayed Al_2O_3 Coatings on Lamellar Structure, *J. Therm. Spray Technol.*, 2004, **13**(3), p 425-431
40. J.-H. Gong, *Fracture Mechanics of Ceramics*, Tsinghua University Press, Beijing, China, 2001 (in Chinese)